To be published in Optics Letters:

Title: Integration of Communication and Distributive Sensing over Optical Supervisory Channel Using Live QPSK Streams

Authors: Maoqi LIU,Jingchuan WANG,Chen Liu,Changyuan Yu,Chao Lu

Accepted: 01 February 25

Posted 03 February 25

DOI: https://doi.org/10.1364/OL.550108

Integration of Communication and Distributed Sensing over Optical Supervisory Channel Using Live QPSK Streams

LIU MAOQI[1,2], WANG JINGCHUAN[1,*], LIU CHEN[2], YU CHANGYUAN[1], AND LU CHAO[1]

[1] Photonics Research Institute, Department of Electrical and Electronic Engineering, The Hong Kong Polytechnic University, Hong Kong, China
[2] National Engineering Laboratory for Next Generation Internet Access System, School of Optical and Electronic Information, Huazhong University of Science and Technology, Wuhan 430074, China
[*] jingchuan98.wang@connect.polyu.hk

Compiled February 1, 2025

The rapid development of wavelength-division multiplexing systems has underscored the critical requirement for effective link monitoring to ensure system reliability and performance. Traditional approaches often rely on separate devices for communication and sensing, which can compromise spectral efficiency and increase system complexity. This work presents an innovative method for integrating communication and sensing within a conventional optical supervisory channel. Four QPSK data streams with different duty ratios enable robust communication and precise sensing with a 125 MBaud transmitter. The forward transmission of communication signals is demonstrated with impeccable accuracy, delivering bit-error-free performance over two fiber links. Concurrently, sensing data is extracted through polarization-diversity reception of the backscattering signal. The distributed acoustic sensing sensitivity achieves 0.50 n$\varepsilon/\sqrt{\text{Hz}}$ in 10.2 km and 0.65 n$\varepsilon/\sqrt{\text{Hz}}$ in 40.0 km at a spatial resolution of 10 m by employing a matched filter. This approach effectively adopts the defined forwarded transmitted control signals or channel information signals, such as channel power, optical signal-to-noise ratio, and Q-factor, simultaneously achieving sensing applications without any dedicated channel or resource.

http://dx.doi.org/10.1364/ao.XX.XXXXXX

Wavelength-division multiplexing (WDM) fiber-optic communication systems provide extensive fiber link resources[1] and numerous network nodes[2] that can be utilized for sensing purposes. Integrating sensing capabilities into communication networks enables diverse applications, such as traffic monitoring[3], perimeter intrusion detection[4], and observing geological phenomena like earthquakes and tsunamis[5–7].

Based on Rayleigh scattering, distributed acoustic sensing (DAS) is a central scheme of backward sensing[8, 9], enabling precise detection of multiple events and subtle changes along the fiber. However, traditional DAS requires a dedicated WDM channel, increasing spectrum resource. Pilot tones have been introduced [10, 11] to achieve integrated sensing and communication (ISAC) in digital subcarrier multiplexing systems, but the power of sensing pilot can degrade communication performance. Alternatively, optical carriers have been utilized for distributed sensing [12], which is restricted to intensity modulation direct detect (IMDD) systems due to the inherent suppression of carriers in coherent optical communication systems. Similarly, both pilot-tone-based and carrier-based ISAC methods require the introduction of additional hardware, such as modulators and optical filters, to generate a pure sensing probe, which significantly increases system complexity and poses challenges for practical deployment. Furthermore, live communication data for distributed sensing have been explored, such as leveraging the backscattering of PSK data to detect vibrations along the fiber link[13]. However, these methods either use continuous signals, which struggle to reconstruct vibration waveforms and only support a sensing range of 500 m[14], or rely on pulse sequences, which are too short to carry sufficient communication information[15].

Optical Supervisory Channel (OSC) offers unique advantages for monitoring within WDM systems. The OSC provides a dedicated channel for communication between network nodes, allowing for both upstream and downstream data transmission independent of the main communication channels[16]. This unique structure makes the OSC highly suitable for sensing applications, as it enables continuous monitoring without interfering with data streaming on the primary communication channels. Surrounding events like hammer strikes can be detected in OSC by monitoring changes in polarization states[17], which has limitations in achieving distributed and precise sensing.

In this letter, a technique is proposed to repurpose the OSC as a combined communication and sensing medium. By adopting a QPSK modulation format and incorporating a designed duty ratio (DR), the forward communication signal with control command or channel information also serves as the sensing probe, akin to a phase-sensitive optical time-domain reflectometry (ϕ-OTDR) system with a long communication frame. The inherently low bandwidth of the OSC aligns well with the sens-

ing system requirements, reducing system complexity and cost. Furthermore, by operating within the OSC, this method circumvents the need to occupy additional frequency or time-domain resources, ensuring compatibility with existing communication fibers. It minimizes cross-channel nonlinear impairments within high-capacity WDM systems, utilizing a matched filter to enhance sensing precision without compromising communication integrity. By meeting both the sensing and communication demands within a unified channel, this technique provides a streamlined and cost-effective solution for real-time network monitoring.

Fig. 1(a) demonstrates the proposed OSC multiplexing scheme in the WDM system. By expanding the functionality of this channel to include Rayleigh backscattering (RBS) sensing, we transform it into a dual-purpose channel, supporting both fiber communication and sensing. This dual-function design effectively leverages existing network infrastructure, eliminating the need for additional sensing channels and minimizing resource overhead. Fig. 1(b) provides a schematic of the structure of the OSC subsystem, showing how the upstream and downstream wavelength channels are organized to supervise the signal-to-noise ratio (SNR) of the channel and convey the information, including Erbium-doped fiber amplifier (EDFA) operating status.

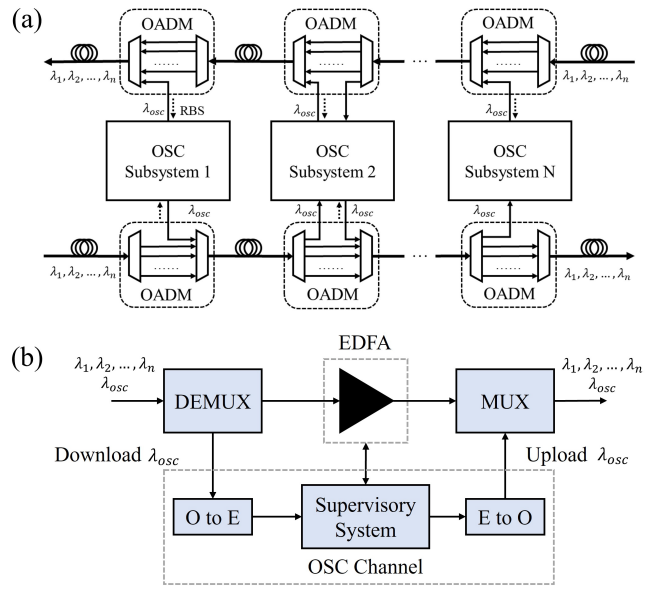

Fig. 1. (a) Proposed OSC scheme in WDM system, and (b) structure of a detailed OSC subsystem.

The primary objective of distributed sensing is to acquire the time response of the optical fiber link, which can be written as $h(t)$. Ideally, the probe distributed detection can be represented by an impulse function $\delta(t)$, and the received signal $r_{\text{ideal}}(t)$ can be expressed as

$$r_{\text{ideal}}(t) = \delta(t) * h(t) = h(t), \tag{1}$$

where the operator '$*$' represents the convolution operation. This means the detection system can identify the instantaneous response at any point along the fiber, thereby achieving high spatial resolution. However, traditional distributed sensing typically employs a single pulse with a certain width τ as the probe signal rect $\left(\frac{t}{\tau}\right)$, where the pulse width directly influences the spatial resolution of the detection. The received signal $r_{\text{pulse}}(t)$ can be expressed as

$$r_{\text{pulse}}(t) = \text{rect}\left(\frac{t}{\tau}\right) * h(t). \tag{2}$$

In distributed sensing based on the communication data stream, communication data symbols are transmitted, which can be seen as a series of pulses. When these symbols reach the receiving end, the received signal is actually the superposition of the time responses of each symbol. The data symbols can be defined as

$$C(t) = \sum_{n=1}^{N} C_n \exp\left(j2\pi f_0 n\tau + j\phi_i\right) \text{rect}\left(\frac{t - n\tau_c}{\tau_c}\right), \tag{3}$$

where C_n means the amplitude of n^{th} single symbol, N is the symbol number, f_0 represents the modulation frequency, τ_c is the duration time of single symbol, ϕ_i is the modulated phase states($i = 1, 2, 3, 4$ for QPSK signal). Then the received signal $r_{\text{comm}}(t)$ can be expressed as

$$r_{\text{comm}}(t) = C(t) * h(t). \tag{4}$$

To extract individual information from each symbol, autocorrelation analysis can be employed to attain the desired time-domain response. Specifically, the received response signal can be correlated with the transmitted symbol signals, which can be expressed as

$$r_{xc}(t) = r_{\text{comm}}(t) \otimes C(t) = [C(t) \otimes C(t)] * h(t), \tag{5}$$

where $r_{xc}(t)$represents the recovered response, and the operator '$\otimes$' represents the correlation operation. The autocorrelation function of data streams can be defined as $k(t) = C(t) \otimes C(t)$, and can be further expressed as

$$k(t) = \Lambda\left(\frac{t}{\tau_c}\right) + n(t) \approx \Lambda\left(\frac{t}{\tau_c}\right), \tag{6}$$

where $\Lambda\left(\frac{t}{\tau_c}\right) = \text{rect}\left(\frac{t}{\tau_c}\right) * \text{rect}\left(\frac{t}{\tau_c}\right)$, $n(t)$ represents the sidebands of the autocorrelation function. In random QPSK signals, the peak-to-sideband noise ratio exceeds 15 dB, which can be neglected in short-distance transmission. Thus, the decoded process can be viewed as using the autocorrelation peak function as a sensing probe. The main lobe width of the function is governed by τ_c, which determines the spatial resolution. The common OSC optical module operates at a 125 MBaud, corresponding to a theoretical spatial resolution of 4 m after rotate-vector summed (RVS)[18]. The complete process of distributed sensing using live QPSK streams is shown in Fig. 2. In this setup, the data symbols go through pulse-shaping to preserve the fidelity of the signal over the fiber link. The signal after pulse shaping can be seen as $C(t)$, and then zero-padding is applied to extend the symbols by adding a series of zero values to the end. The length of the zero-padding is chosen to be greater than the round-trip time (RTT) of the fiber under test (FUT) to prevent overlap between consecutive sequences. Meanwhile, the length of symbols in each data stream must be less than the zero-padding length to avoid autocorrelation interference between consecutive sequences. The structured sequence is sent to an arbitrary waveform generator (AWG) for up-sampling to prevent inter-symbol interference and transmission through the FUT. The data streams propagate forward as a communication signal while simultaneously enabling sensing based on its

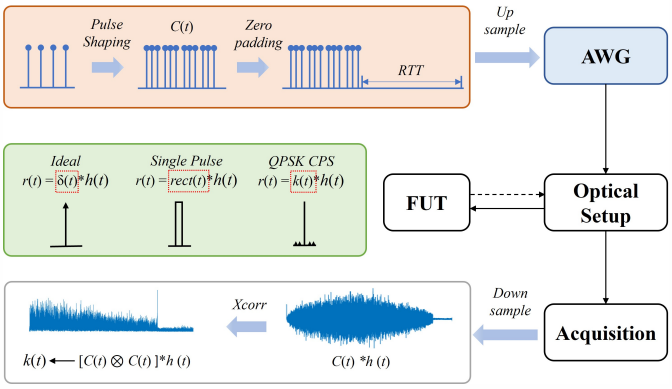

Fig. 2. Process of distributed sensing using live QPSK streams.

backscattered reflection. Finally, the sensing signal is collected by the acquisition system and downsampled, and then the cross-correlation is performed to isolate the backscattering sensing information from the forward communication signal.

We conduct a 125 MBaud QPSK experiment to demonstrate the proposed ISAC scheme over OSC, as illustrated in Fig. 3. An AWG (Keysight M8190A) generates four communication streams with different DRs. To satisfy the previously mentioned zero-padding condition, the duration time without information is set to be longer than one RTT, specifically 2^{14} symbols for 10.2-km fiber and 2^{16} symbols for 40.0-km fiber. Four QPSK streams with DRs of 5.9%, 20.0%, 33.3%, and 50.0% are transmitted over two fiber links. The light emitted from the narrow linewidth laser (NKT E15) is equally divided into two paths: one path is directed to the IQ modulator, and the other path serves as the local oscillator. EDFA1 and EDFA2 are used to amplify the communication and backscattering sensing signals. After amplifying, two optical bandpass filters (OBPFs) filtered out unwanted spontaneous emission (ASE) noise. A 10 m piezoelectric ceramic transducer (PZT), driven by a sin wave of 800 mV Vpp and 200 Hz frequency, is placed at the end of the fiber link to test vibration. The communication signal is received by four balanced photodetectors (BPDs) and a digital storage oscilloscope (DSO, Keysight DSAZ594A). On the communication side, it is essential to first trim the resampled signal since the transmitted signal is structured with a specific DR. It involves isolating the valuable information by discarding the zero-padded portions and then continuing the subsequent compensation steps (chromatic dispersion compensation, frequency offset compensation, and carrier phase recovery). On the sensing side, polarization-diverse reception of the Rayleigh backscattering signal is implemented to eliminate polarization fading with the integrated, coherent receiver (ICR, Neophotonic class 40), followed by another DSO (Keysight MSOS404A). To mitigate interference fading, we apply the RVS algorithm based on the communication signal, which utilizes a Finite Impulse Response (FIR) filter to divide the spectrum of the transmitted non-return-to-zero (NRZ) signal into five distinct segments. Subsequently, a low-pass filter is applied to the demodulated trace in the time domain, resulting in a smoothed phase trace.

Figure 4(a) and (b) show the demodulated phase traces received for streams with DRs of 5.9% and 50.0% over a 10.2-km fiber link. For the low DR stream, the location of the vibration point can be accurately identified and a spatial resolution of 10 m can be determined from the zoom-in view of Fig. 4(a).

However, as the DR increases, phase noise becomes more

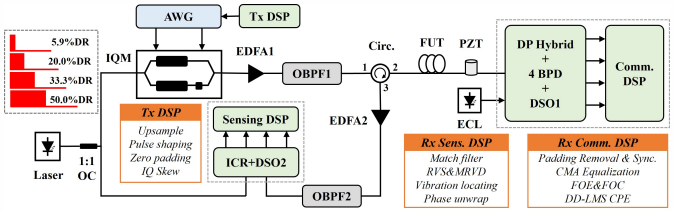

Fig. 3. 125 MBaud QPSK ISAC Experimental setup.

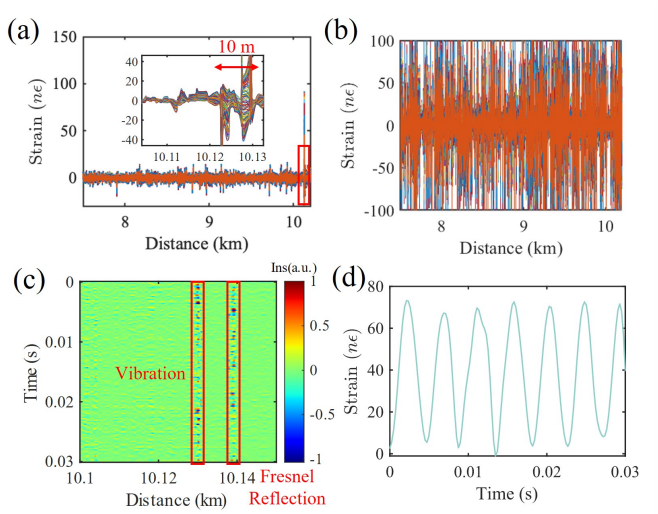

Fig. 4. Strain traces of (a) 5.9% DR stream and (b) 50.0% DR stream. (c) Differential intensity plot and (d) extracted strain trace of 50.0% DR stream.

pronounced, making it challenging to locate the vibration points for long-sequence QPSK streams. Although we have already significantly suppressed interference and polarization fading effects employing the RVS algorithm and dual-polarization receivers, the noise in these longer sequences primarily arises from non-ideal autocorrelation properties of the probe signal $k(t)$. As the DR grows, the noise side-lobes $n(t)$ in the autocorrelation function have a broader influence, leading to phase trace overlap and reduced clarity.

Despite this, the strong autocorrelation peak $\Lambda(t)$ generated by the probe sequence remains sufficient to excite a robust channel response in terms of signal intensity. Subsequently, we can identify the vibration locations by analyzing the intensity waterfall plot rather than relying on the phase waterfall. Taking the 50.0% DR stream as an example, Fig. 4(c) displays the intensity distribution relative to the initial time, where vibration and Fresnel reflection locations are distinguishable. Fig. 4(d) illustrates the extracted strain waveform from the identified location, and the PSD curves of the extracted vibration waveforms from four sets of streams are calculated in Fig. 5(a). The PSD curves indicate that the frequency of the demodulated vibration is approximately 200 Hz, with a noise floor of about -28 dB rad^2/Hz. The corresponding strain sensitivity is calculated to be 0.50 n$\varepsilon/\sqrt{\text{Hz}}$, which determines the lower limit of strain detection. The experiment is subsequently extended to a 40.0-km fiber link. Under this condition, the accumulation of laser phase noise over the extended distance, combined with the limitations of the correlation function, resulted in the loss of vibration information in streams with 33.3% and 50.0% DRs.

The sensing performance of the system with 20.0% DR stream at different PZT vibration frequencies is further tested, with the corresponding PSD curves presented in Fig. 5(b). The noise floor of the PSD curves is about -25 dB rad^2/Hz, corresponding to a strain sensitivity of 0.65 n$\varepsilon/\sqrt{\text{Hz}}$. The maximum detectable vibration frequency is intrinsically linked to the sensing distance and stream DR due to its impact on the sampling rate of the event.

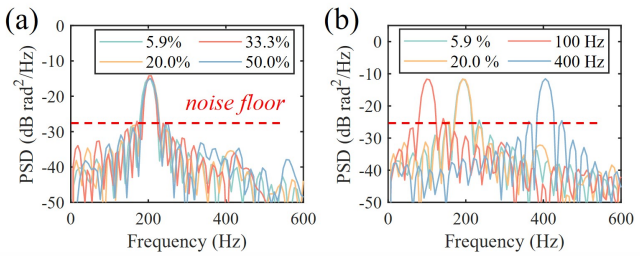

Fig. 5. (a) The PSD curves of different DR streams over 10.2-km fiber link. (b)The PSD curves of 5.9% and 20.0% DR streams and different vibration frequencies adopting 20.0% DR over 40.0-km fiber link.

The SNR of the proposed system is calculated as the ratio of the root-mean-square (RMS) strain value at the location of the PZT to that of the calm fiber section wound around the PZT. Table 1 shows the SNR values for DRs and fiber lengths. Regarding the distributed sensing of 10.2-km fiber, SNR decreases steadily as DR increases. For the 40.0-km fiber, SNR drops sharply at higher DRs, and vibration information is unobtainable beyond 20.0% DR due to excessive noise.

Table 1. SNR under different DRs and fiber lengths

Fiber Length	SNR under different DRs (dB)			
	5.9%	20.0%	33.3%	50.0%
10.2 km	18.81	14.80	11.63	4.24
40.0 km	16.70	5.55	-	-

Fig. 6(a) depicts the SNR of the demodulated signals at the communication receiver under the transmission of four sets of sequences, with no bit errors (BER) observed over the entire 10.2-km and 40.0-km fiber link. The stream with low DR means higher peak power launched into the fiber induces nonlinear effects in the channel during long-distance transmission, impacting communication performance. Consequently, under the 40.0-km link, the SNR of the stream with a 5.9% DR exhibits a significant decline. Fig. 6(b) and (c) illustrate the communication constellations for transmissions at 20.0% DR over 10.2-km and 40.0-km fiber links, demonstrating that the extended transmission distance minimally impacts communication performance. Based on the calculated sensing SNR and communication performance, the QPSK stream with a 20.0% DR is preferred. It represents the maximum duty cycle that allows for effective distributed sensing, achieving the trade-off between increased communication rate and sensing capability over 40.0-km transmission.

In conclusion, the integrated system effectively combines communication and sensing within OSC through live QPSK

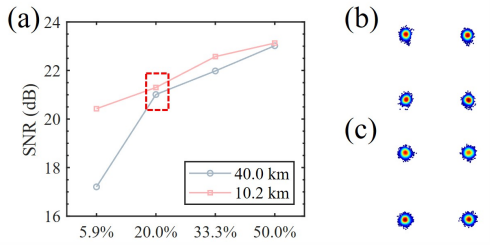

Fig. 6. (a) SNR and of the forward communication signals over two fiber links. Constellations for transmissions at 20.0% DR over (b) 10.2 km and (c) 40.0 km.

streams. Distributed vibration sensing and forward communication with 125 MBaud QPSK streams with four different DRs are demonstrated over 10.2-km and 40.0-km fiber links. By integrating intensity plots for localization with phase traces for strain demodulation, six out of the eight setups successfully achieve distributed sensing. Our approach provides a scalable solution for network operators, enhancing channel utility and supporting real-time monitoring applications without additional infrastructure.

Funding. Hong Kong Government (HK RGC GRF 15209321 B-Q85G); National Key Research and Development Program of China (2023YFB2905300).

Disclosures. The authors declare no conflicts of interest.

Data Availability. Data underlying the results presented in this paper are not publicly available at this time but may be obtained from the authors upon reasonable request.

REFERENCES

1. E. Ip, J. Fang, Y. Li, *et al.*, J. Opt. Commun. Netw. **14**, A61 (2022).
2. Y.-K. Huang and E. Ip, "Simultaneous optical fiber sensing and mobile front-haul access over a passive optical network," in *2020 OFC,* (2020), pp. 1–3.
3. M.-F. Huang, M. Salemi, Y. Chen, *et al.*, J. Light. Technol. **38**, 75 (2020).
4. G. A. Wellbrock, T. J. Xia, M.-F. Huang, *et al.*, J. Light. Technol. **41**, 3758 (2023).
5. G. Marra, C. Clivati, R. Luckett, *et al.*, Science **361**, 486 (2018).
6. Z. Zhan, M. Cantono, V. Kamalov, *et al.*, Science **371**, 931 (2021).
7. G. Marra, D. M. Fairweather, V. Kamalov, *et al.*, Science **376**, 874 (2022).
8. C. Dorize, S. Guerrier, E. Awwad, and J. Renaudier, "Capturing acoustic speech signals with coherent mimo phase-otdr," in *2020 ECOC,* (2020), pp. 1–4.
9. G. A. Wellbrock, T. J. Xia, M.-F. Huang, *et al.*, "First field trial of sensing vehicle speed, density, and road conditions by using fiber carrying high speed data," in *2019 OFC,* (2019), pp. 1–3.
10. B. Yang, J. Tang, C. Cheng, *et al.*, J. Light. Technol. pp. 1–7 (2024).
11. Z. Hu, M. Zhang, Y. Li, *et al.*, Opt. Lett. **49**, 3166 (2024).
12. H. He, L. Jiang, Y. Pan, *et al.*, Light. Sci. Appl. 2023 12:1 **12**, 1 (2023).
13. H. Martins, K. Shi, B. Thomsen, *et al.*, Opt. Express **24**, 22303 (2016).
14. H. F. Martins, K. Shi, B. C. Thomsen, *et al.*, "Code length limit in phase-sensitive otdr using ultralong (>1m bits) pulse sequences due to fading induced by fiber optical path drifts," in *2017 OFS,* (2017), pp. 1–4.
15. P. Li, Y. Wang, X. Liu, *et al.*, J. Light. Technol. **41**, 3225 (2023).
16. G. Ellinas, D. Papadimitriou, J. Rak, *et al.*, Opt. Switch. Netw. **14**, 179 (2014).
17. J. E. Simsarian and P. J. Winzer, "Shake before break: Per-span fiber sensing with in-line polarization monitoring," in *2017 OFC,* (2017), p. M2E.6.
18. D. Chen, Q. Liu, and Z. He, Opt. Express **25 7**, 8315 (2017).

FULL REFERENCES

1. E. Ip, J. Fang, Y. Li, *et al.*, "Distributed fiber sensor network using telecom cables as sensing media: technology advancements and applications [invited]," J. Opt. Commun. Netw. **14**, A61–A68 (2022).
2. Y.-K. Huang and E. Ip, "Simultaneous optical fiber sensing and mobile front-haul access over a passive optical network," in *2020 OFC,* (2020), pp. 1–3.
3. M.-F. Huang, M. Salemi, Y. Chen, *et al.*, "First field trial of distributed fiber optical sensing and high-speed communication over an operational telecom network," J. Light. Technol. **38**, 75–81 (2020).
4. G. A. Wellbrock, T. J. Xia, M.-F. Huang, *et al.*, "Explore benefits of distributed fiber optic sensing for optical network service providers," J. Light. Technol. **41**, 3758–3766 (2023).
5. G. Marra, C. Clivati, R. Luckett, *et al.*, "Ultrastable laser interferometry for earthquake detection with terrestrial and submarine cables," Science **361**, 486–490 (2018).
6. Z. Zhan, M. Cantono, V. Kamalov, *et al.*, "Optical polarization–based seismic and water wave sensing on transoceanic cables," Science **371**, 931–936 (2021).
7. G. Marra, D. M. Fairweather, V. Kamalov, *et al.*, "Optical interferometry–based array of seafloor environmental sensors using a transoceanic submarine cable," Science **376**, 874–879 (2022).
8. C. Dorize, S. Guerrier, E. Awwad, and J. Renaudier, "Capturing acoustic speech signals with coherent mimo phase-otdr," in *2020 ECOC,* (2020), pp. 1–4.
9. G. A. Wellbrock, T. J. Xia, M.-F. Huang, *et al.*, "First field trial of sensing vehicle speed, density, and road conditions by using fiber carrying high speed data," in *2019 OFC,* (2019), pp. 1–3.
10. B. Yang, J. Tang, C. Cheng, *et al.*, "Integrated communication and enhanced forward phase-based sensing based on frequency-domain pilot tones in dscm systems using 100 khz ecls," J. Light. Technol. pp. 1–7 (2024).
11. Z. Hu, M. Zhang, Y. Li, *et al.*, "Enabling endogenous distributed acoustic sensing in a digital subcarrier coherent transmission system," Opt. Lett. **49**, 3166–3169 (2024).
12. H. He, L. Jiang, Y. Pan, *et al.*, "Integrated sensing and communication in an optical fibre," Light. Sci. Appl. 2023 12:1 **12**, 1–14 (2023).
13. H. Martins, K. Shi, B. Thomsen, *et al.*, "Real time dynamic strain monitoring of optical links using the backreflection of live psk data," Opt. Express **24**, 22303–22318 (2016).
14. H. F. Martins, K. Shi, B. C. Thomsen, *et al.*, "Code length limit in phase-sensitive otdr using ultralong (>1m bits) pulse sequences due to fading induced by fiber optical path drifts," in *2017 OFS,* (2017), pp. 1–4.
15. P. Li, Y. Wang, X. Liu, *et al.*, "Quadrature phase-shift keying modulation with random coding pulse for long-range ϕ-otdr," J. Light. Technol. **41**, 3225–3233 (2023).
16. G. Ellinas, D. Papadimitriou, J. Rak, *et al.*, "Practical issues for the implementation of survivability and recovery techniques in optical networks," Opt. Switch. Netw. **14**, 179–193 (2014).
17. J. E. Simsarian and P. J. Winzer, "Shake before break: Per-span fiber sensing with in-line polarization monitoring," in *2017 OFC,* (2017), p. M2E.6.
18. D. Chen, Q. Liu, and Z. He, "Phase-detection distributed fiber-optic vibration sensor without fading-noise based on time-gated digital ofdr." Opt. Express **25 7**, 8315–8325 (2017).